ACS NANO
Cite This: ACS Nano XXXX, XXX, XXX–XXX
www.acsnano.org

ARTICLE

Experimental Demonstration of Hyperbolic Metamaterial Assisted Illumination Nanoscopy

Qian Ma,[†] Haoliang Qian,[†] Sergio Montoya,[†] Wei Bao,[‡] Lorenzo Ferrari,[§,∥] Huan Hu,[†] Emroz Khan,[⊥] Yuan Wang,[‡] Eric E. Fullerton,[†,§] Evgenii E. Narimanov,[⊥] Xiang Zhang,[‡] and Zhaowei Liu*[,†,§,∥]

[†]Electrical and Computer Engineering, University of California, San Diego, 9500 Gilman Drive, La Jolla, California 92093, United States

[‡]Mechanical Engineering, University of California, Berkeley, 5130 Etcheverry Hall, Berkeley, California 94720, United States

[§]Center for Memory and Recording Research, University of California, San Diego, 9500 Gilman Drive, La Jolla, California 92093, United States

[∥]Material Science and Engineering, University of California, San Diego, 9500 Gilman Drive, La Jolla, California 92093, United States

[⊥]School of Electrical Engineering and Birck Nanotechnology Center, Purdue University, West Lafayette, Indiana 47907, United States

Supporting Information

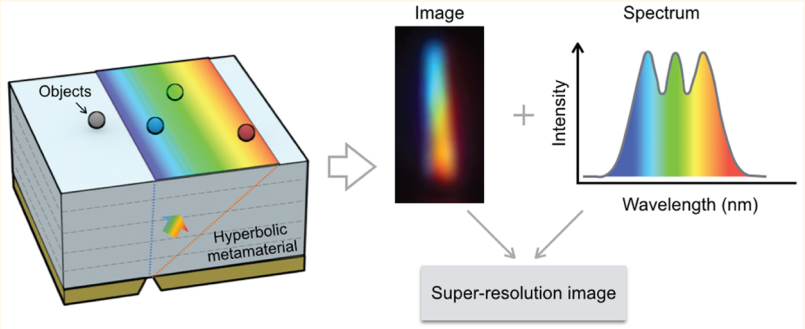

ABSTRACT: **An optical metamaterial is capable of manipulating light in nanometer scale that goes beyond what is possible with conventional materials. Taking advantage of this special property, metamaterial-assisted illumination nanoscopy (MAIN) possesses tremendous potential to extend the resolution far beyond conventional structured illumination microscopy. Among the available MAIN designs, hyperstructured illumination that utilizes strong dispersion of a hyperbolic metamaterial (HMM) is one of the most promising and practical approaches, but it is only theoretically studied. In this paper, we experimentally demonstrate the concept of hyperstructured illumination. A ~80 nm resolution has been achieved in a well-known Ag/SiO_2 multilayer HMM system by using a low numerical aperture objective (NA = 0.5), representing a 6-fold resolution enhancement of the diffraction limit. The resolution can be significantly improved by further material optimization.**

KEYWORDS: *super-resolution, hyperbolic metamaterial, structured illumination microscopy, nanofabrication, plasmonics*

The conventional optical microscope has its resolution limit at one-half of the wavelength due to the diffraction of light. Modern super-resolution techniques, including single-molecule localization microscopy[1−3] and stimulated emission depletion microscopy,[4] overcome the limit by taking advantages of the fluorescing mechanism. Although their resolution could be ultrahigh (sub-10 nm),[5] the speed or phototoxicity must be compromised. Structured illumination microscopy (SIM),[6,7] on the other hand, combines wide-field capability, high frame rate, and low phototoxicity, leading to wide adoption in super-resolution applications. However, its resolution is typically limited at twice the diffraction limit.

Metamaterials provide an alternative solution for super-resolution that does not necessarily rely on fluorescence.

Received: August 8, 2018
Accepted: October 17, 2018
Published: October 17, 2018

DOI: 10.1021/acsnano.8b06026
ACS Nano XXXX, XXX, XXX–XXX

Initiated from the theoretical *perfect lens*,[8] a number of superlens and hyperlens demonstrations can be found.[9−16] Those metamaterial-based lenses have shown promising subdiffraction resolution[17] and have covered a broad range of operation frequency.[18] Despite that, it is still challenging to apply an optical metamaterial lens in a practical imaging scenario. First, a hyperlens[11,12] requires a curved geometry to gain optical magnification, resulting in a limited field of view. Although the flat version of a hyperlens is proposed based on transformation optics,[19,20] the experiment has not yet been demonstrated due to the complexity in fabrication. Second, metamaterial at optical frequency usually is made by compositing a dielectric and a metal. Metallic losses of metamaterial-based lenses result in higher photon dosage to the object to maintain a reasonable signal to noise ratio, which might not fit well to applications such as bioimaging.

To overcome the limitation of the aforementioned metamaterial lenses, one of the approaches is to combine a metamaterial with the structured illumination method, which can be named as metamaterial-assisted illumination nanoscopy (MAIN).[21] This method uses a flat metamaterial (could be an array of slits in a metallic film,[22] an array of plasmonic structures,[23] a nanopatterned hyperbolic metamaterial,[24,25] or graphene[26]), serving as a sample holder/substrate instead of a lens, to transform the incident light into structured illumination patterns that are far beyond the traditional diffraction limit. Thus, it can dramatically increase the resolution of SIM and also keep the inherent advantage of SIM including low phototoxicity and high imaging speed. Moreover, the metamaterial will interact with the specimen, causing enhanced Raman scattering,[27] enhanced fluorescent lifespan,[28] and second-harmonic generation,[29] which are potentially beneficial in certain applications such as label-free imaging or longtime fluorescent imaging.

Among the existing designs of MAIN, using a hyperbolic metamaterial provides the most promising resolution in theory. A recent theoretical study introduces hyperstructured illumination,[24] which uses a highly dispersive hyperbolic metamaterial (HMM) to project a series of wavelength-dependent sub-diffraction-limited illumination patterns. This method maps the high-resolution spatial information to a spectrum that can be collected at far field and can be further combined with a compressive sensing imaging method.[25]

In this paper, we experimentally demonstrate the hyperstructured illumination by using a Ag/SiO_2 multilayer HMM. We verify that, by using a nanoslit on HMM, the HMM can perform a one-dimensional mapping from spatial locations in subdiffraction scale to a spectrum as predicted in ref 24. Then we use the far-field-collected spectral data to reconstruct super-resolution surface images, achieving ~80 nm resolution, which is far beyond the diffraction limit of the collection objective with NA = 0.5. This study is an experimental demonstration of the MAIN concept using a hyperbolic metamaterial.

RESULTS

Hyperstructured Illumination. HMMs used in hyperstructured illumination have two functions: they provide deep-subwavelength-scale illumination at near field; they are highly dispersive so that the wavelength can be used to control the illuminated location. An HMM has its iso-frequency curve in a hyperbolic shape:

$$\frac{k_x^2}{\varepsilon_z} + \frac{k_z^2}{\varepsilon_x} = k_0^2 \tag{1}$$

where $\varepsilon_x < 0$, $\varepsilon_z > 0$ (type-II HMM) are the elements of the HMM permittivity tensor and k_0 is the wave vector in air.

The direction θ of group velocity v_g is normal to the hyperbolic isofrequency curve. When $k_x \gg k_0$, it yields

$$\theta \approx \arctan\sqrt{-\varepsilon_x/\varepsilon_z} \tag{2}$$

The angles of group velocity θ are almost independent of k_x. Therefore, a beam incoupled from a narrow slit will not diverge when it is propagating inside an HMM (Supporting Figure 1). The propagating angle θ can be tuned by input wavelength due to the strong wavelength dependence of the effective permittivity ε_x and ε_z (Supporting Figure 2).

Benefiting from the directional propagation and strong dispersion, when the broadband light is injected through a narrow-slit mask on one side of the HMM, the HMM, like a grating, spreads the beam based on wavelength and redistributes it to the other side of the HMM. For each wavelength, the beam remains well-confined. Therefore, with the help of a nanoslit coupler, a flat type-II HMM maps spatial information at the nanoscale to a spectrum. This phenomenon is first applied to lithography,[30] then for the hyperstructured illumination. It should be noted that there are two symmetrical beams from a single slit (see Supporting Figure 1). For simplicity, we discuss only one of the two beams in the following sections.

Figure 1 illustrates our experimental setup of hyperstructured illumination. The system consists of a test sample for hyperstructured illumination, a transmission mode dark-field microscope, a broadband light source, and a tunable bandpass filter to measure spectral data. The HMM substrate, when illuminated by white light, projects sub-diffraction-limited wavelength-dependent patterns onto the object that lies at its top surface. The object, interacting with those near-field patterns, scatters light to the far field, which is later collected by diffraction-limited optics,

$$I(\boldsymbol{r}, \lambda) = P(\boldsymbol{r}, \lambda)\, O(\boldsymbol{r}, \lambda) \otimes \mathrm{PSF}(\boldsymbol{r}, \lambda) \tag{3}$$

where I is the hyperspectral image, P is the near-field illumination patterns, O is the object, and PSF is the point spread function of the imaging system. Therefore, the object O can be retrieved by the spectral data I with known illumination patterns P. In this specific case when a single nanoslit is used to in-couple illumination, $P(\boldsymbol{r}, \lambda)$ looks like a nanoscale "rainbow" with its size and wavelength dependency determined by the dispersion of the HMM.

In hyperstructured illumination, the two-dimensional object function $O(x, y)$ is defined by a Motti projection[24] of the spatial distribution of the dielectric permittivity of the actual object, $\varepsilon(x, y, z)$, as

$$O(x, y) = \frac{1}{2\pi} \int \mathrm{d}x' \int \mathrm{d}y' \int \mathrm{d}z' \times \frac{z'(\varepsilon(x', y', z') - 1)}{((x - x')^2 + (y - y')^2 + (z - z')^2)^{3/2}} \tag{4}$$

which not only "projects" the imaging target onto the object plane $z = 0$, but also visualizes its full three-dimensional structure. This behavior is illustrated in Figure 2, which shows three examples of an actual object (the word "Abbe" formed by

DOI: 10.1021/acsnano.8b06026
ACS Nano XXXX, XXX, XXX−XXX

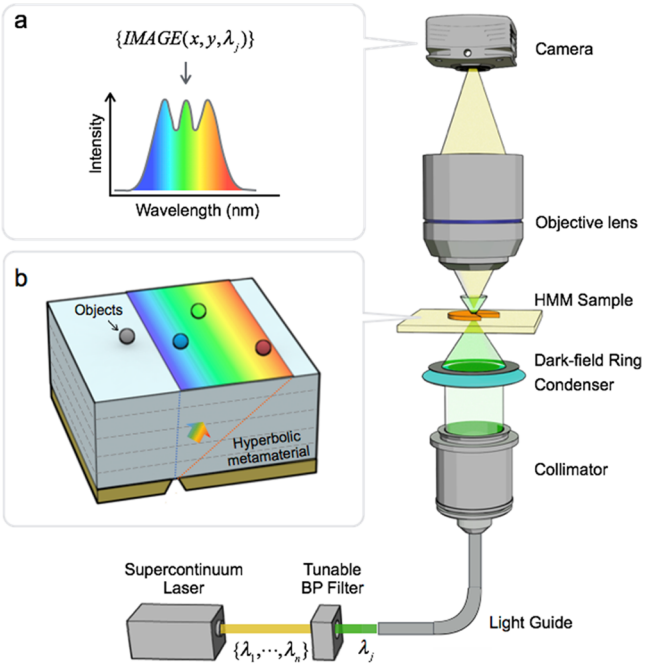

Figure 1. Hyperstructured illumination and its experimental setup. The hyperbolic metamaterial (HMM) sample is imaged under a conventional microscope in dark-field configuration. A supercontinuum laser, equipped with a tunable bandpass filter, which serves as a light source, scans its output wavelength from 460 to 840 nm in series, while the HMM sample is imaged by a camera to form a hyperspectral image $I(x, y, \lambda)$. The dark-field mode ensures that only scattered signal (drawn in light yellow) from the objects (on top of the HMM sample) is collected. (a) Scattering signal from particles at different positions have a different wavelength, respectively. (b) The hyperstructured illumination device has incoming light coupled through a nanoslit. The HMM then projects a nanoscale "rainbow" on its top surface to illuminate the object.

solid 3D letters of various heights, etched in a dielectric surface) and the corresponding Motti projection. Note that the changes in intensity of the image represent the differences in the variations of the local height of the object in the z-direction.

Sample Preparation. The test sample of hyperstructured illumination consists of a layer of Cr mask, an HMM made by multiple pairs of Ag and SiO_2, and a Si_3N_4 layer serving as an object, as illustrated in Figure 3a. The fabrication process starts from a Si_3N_4 membrane window (Figure 3b). Six pairs of Ag/SiO_2 (thickness per layer: 14 nm, ratio: 1:1) is deposited on the 50 nm thick Si_3N_4 membrane. Then the HMM is covered by a 40 nm Cr layer. All layers are deposited by magnetron sputtering. The quality of the hyperbolic metamaterial is examined by imaging its cross-section by FIB-SEM. The Ag and SiO_2 layers are well separated from each other (Figure 3c). The same focused ion beam (FIB) is used to make nanoslits on both sides of the sample. Straight lines (~few micrometers long) are milled on the Cr mask to couple light into the HMM. The SEM image of the milled straight line shows a line width of ~27 nm (Figure 3d). The 50 nm thick Si_3N_4 layer is used as the artificial object layer. Two different objects are milled into it by FIB to demonstrate the performance of hyperstructured illumination in the following two sections.

Verification of the HMM Dispersion. The first artificial object is designed to experimentally measure spatial-spectral mapping: the relationship between the illuminated position and the incident wavelength. This spatial-spectral mapping is mainly determined by the dispersive permittivity of the HMM. A ~10 μm long line is milled into a Si_3N_4 membrane to interact with one of the two symmetrical near-field "rainbow" patterns generated by the single nanoslit in the Cr mask. A small tilting angle (α = 1.51 degree) between the slits on either side of the HMM makes separation d changes along the y direction, as illustrated in Figure 4a and imaged by a scanning electron microscope (SEM) in Figure 4c. The sample is measured by a dark-field microscope shown in Figure 1 (see Methods/Experimental for setup details). Based on the HMM dispersion property, as d increases, the spectrum of this tilted line shifts to longer wavelength. This phenomenon is first observed from an RGB image (Figure 4b) in the far field and

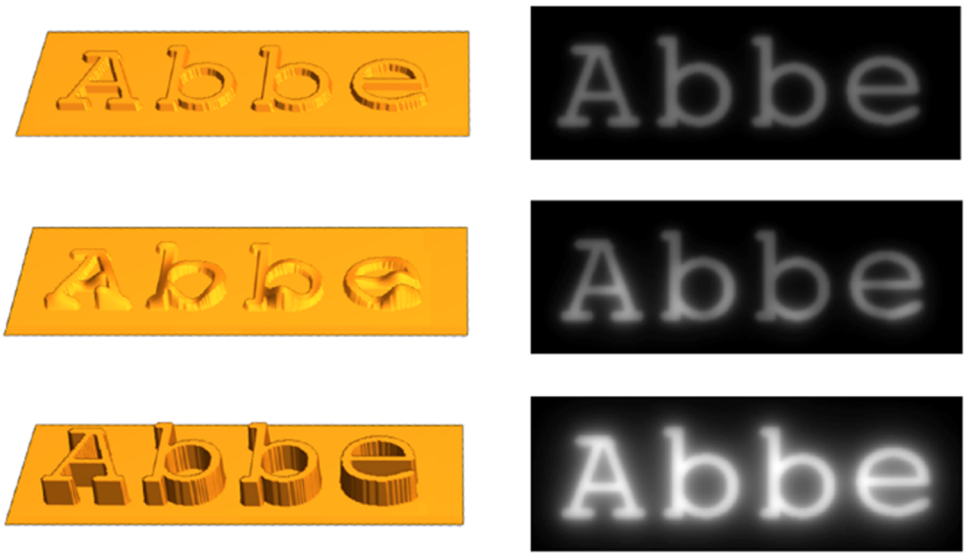

Figure 2. Motti projection. Three examples of a solid object: the word "Abbe" etched in a dielectric surface, with different variations of the height of the letters (left column), and the corresponding Motti projections. Note that an increase in height of the object leads to an increase in the brightness of the image at the corresponding location.

DOI: 10.1021/acsnano.8b06026
ACS Nano XXXX, XXX, XXX−XXX

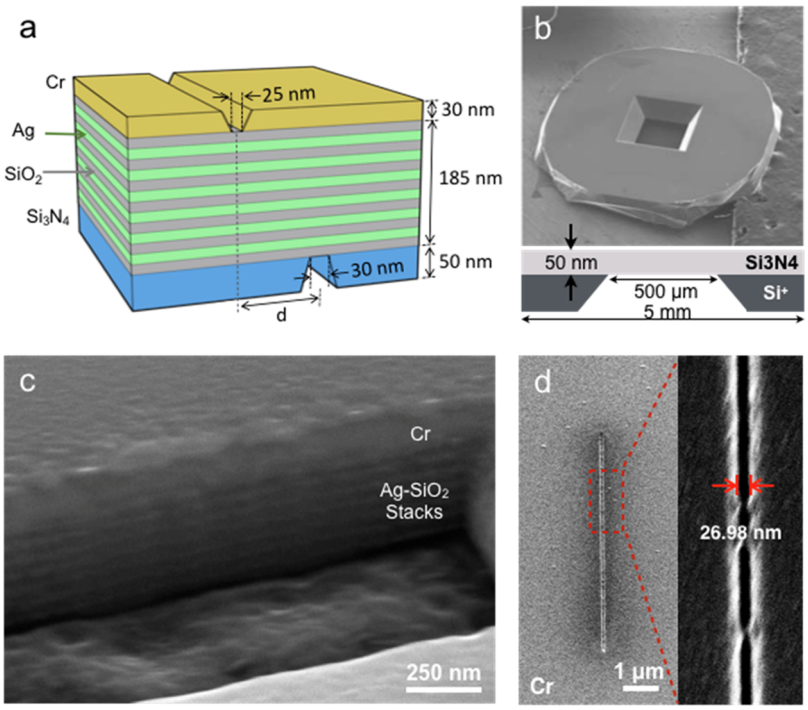

Figure 3. Sample preparation. (a) Schematics of a multilayer HMM deposited on a Si_3N_4 membrane window. The multilayer consists of Ag−SiO_2 stacks (6 pairs; thickness of each layer, 14 nm). Air slits in the Cr mask and Si_3N_4 membrane are made by FIB. The width of the air slit is ∼25 nm on the Cr side and ∼30 nm on the Si_3N_4 side. The distance d varies from 350 to 550 nm. (b) Sketch and SEM image of a Si_3N_4 membrane window. The window size is 0.5 mm. The membrane thickness is 50 nm. (c) FIB-SEM cross-section image of Ag−SiO_2 stacks. (d) SEM image of a 10 μm long slit on the Cr side.

then quantitatively analyzed by measuring the spectral shifts of the titled line along the y direction (Figure 4d).

The spectrum is measured by first taking a diffraction-limited spectral image,

$$I(x, y, \lambda) = O(x, y)\, P(x, \lambda) \otimes \mathrm{PSF}(x, y) \tag{5}$$

then integrating along the x direction,

$$S(\lambda, y) = \int I(x, y, \lambda)\, \mathrm{d}x \tag{6}$$

The hyperspectral image is taken by stepping the tunable bandpass filter from 460 nm to 840 nm with steps of 10 nm. Selected spectra at indicated locations are plotted in Figure 4d. For each spectrum in $S(\lambda, y)$, we find the peak wavelength and plot it as a function of separation d based on the known geometrical relationship between y and d.

$$\Delta d = \Delta y\, \Delta\tan(\alpha) \tag{7}$$

A red shift of spectral peaks can be observed when y (and d) increases, which stands for the spatial-spectral mapping of this specific device. The measured peak locations (red circles) agree well with the predictions (blue dashed line) from simulation, while the small deviations may come from the nonideal sample quality. This experiment, by using a prior known object, proves that the dispersive material property of the prepared HMM is close to our simulation, and hence, the spatial-spectral mapping in hyperstructured illumination is verified.

Image Reconstruction and Super-Resolution Demonstration. Based on the verified spatial-spectral mapping, we can reconstruct a super-resolution image of an unknown object from its scattered spectral information. Presuming an object is illuminated by the nanorainbow and its scattering images at multiple wavelength are measured at far field in the setup shown in Figure 1, the notation of the measured hyperspectral image can be rewritten as

$$I(x, y, \lambda) = \iint E(x' - D\lambda - x_0)\, O(x', y') \times \mathrm{PSF}(x - x', y - y')\, \mathrm{d}x'\, \mathrm{d}y' \tag{8}$$

where $E(x)$ is the intensity distribution of the well-confined line illumination at a single wavelength on the top surface of the HMM. The illuminated line has wavelength-dependent locations $D\lambda + x_0$, where D and x_0 are fitted parameters from Figure 4d. The reconstruction includes two steps: first, a series of digital apertures is added on every frame of the hyperspectral image; second, all the processed frames are summed to form a super-resolution image:

$$\mathrm{Im}(x, y) = \int I(x, y, \lambda)\, A(x - D\lambda - x_0)\, \mathrm{d}\lambda \approx I\left(x, y, \frac{x - x_0}{D}\right) \tag{9}$$

where A is the digital aperture ($A(x) \approx \delta(x)$) added to every wavelength frame of the spectral image. Substitute eq 8 into eq 9, we obtain

$$\mathrm{Im}(x, y) = \iint E(x' - x)\, O(x', y')\, \mathrm{PSF}(x - x', y - y')\, \mathrm{d}x'\, \mathrm{d}y' \tag{10}$$

$$\mathrm{Im}(x, y) = O(x, y) \otimes \mathrm{PSF}_{\mathrm{eff}}(x, y) \tag{11}$$

$\mathrm{PSF}_{\mathrm{eff}}$ is the effective point spread function,

DOI: 10.1021/acsnano.8b06026
ACS Nano XXXX, XXX, XXX−XXX

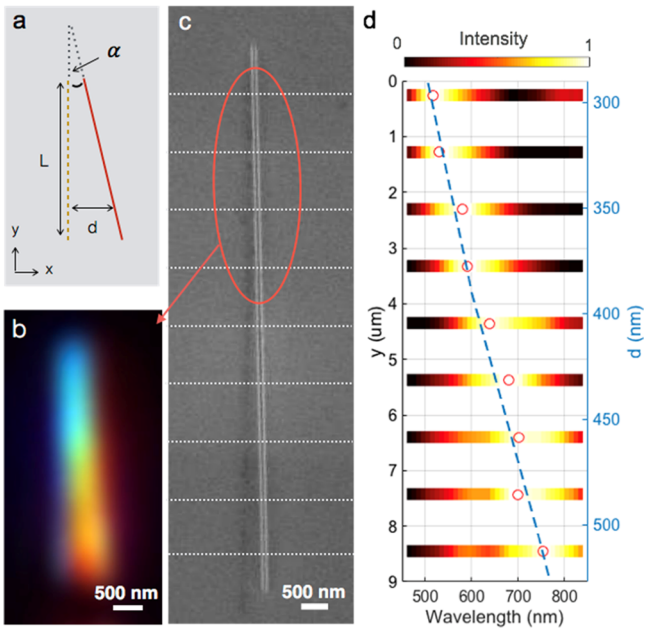

Figure 4. Verification of spatial-spectral mapping. (a) Schematic illustration of the relative location between the coupling slit in the Cr film (dashed yellow line) and the object slit in the Si_3N_4 film (solid red line). The angle α is 1.51 degrees (exaggerated in the drawing). L: 10 μm. (b) Diffraction-limited RGB image of the tilted slit. The three channels (RGB) are acquired in series by setting the tunable bandpass filter to [460 nm: 500 nm], [510 nm: 570 nm], and [580 nm: 700 nm], respectively. (c) Scanning electron microscope (SEM) image of the entire slit in the Si_3N_4 membrane. (d) Spectral response along the y direction (and distance d along the x direction) in (c) at indicated locations (white dashed line). Distance d is calculated based on the known geometrical relationship with y. Red circles: Peak positions of each measured spectrum. Blue dashed line: Full wave simulation of near-field beam locations *versus* wavelength for the same Ag/SiO_2 multilayer.

$$\mathrm{PSF}_{\mathrm{eff}}(x, y) = E(x)\,\mathrm{PSF}(x, y) \tag{12}$$

Since $E(x)$ typically has a much smaller full width at half maximum (FWHM) than the point spread function of a microscope, hyperstructured illumination has great resolution improvement along the x direction. The synchronized scan of the digital aperture and laser focal spot makes the process similar to a confocal laser scan microscope.[31]

To test the imaging resolution, we image a tilted line pair in the Si_3N_4 membrane shown in Figure 5. The objects are made by FIB milling. The spectral image is taken by the same experimental setup used for Figure 4. We use a Zeiss 50×/NA 0.5 objective lens, and hence, the FWHM of the PSF is ~λ. From full wave simulation of the prepared Ag−SiO_2 multilayer HMM, the FWHM of $E(x)$ is ~80 nm (operating wavelength: 500 nm), which mainly determines the resolving power. The dispersion coefficient D is measured to be ~0.81 nm/nm (position/wavelength). The dispersion coefficient D is mainly determined by the number of Ag−SiO_2 pairs and, hence, the total thickness of the multilayer. In the far-field optical measurement, it is hard to precisely know x_0, which is related to the location of the slit on the Cr mask. Fortunately, a small misalignment of x_0 will not affect the resolving power.[31] For the imaging reconstruction in Figure 5, a scan of x_0 is performed, and the final x_0 is manually selected based on the quality of the reconstructed images. As observed from the SEM

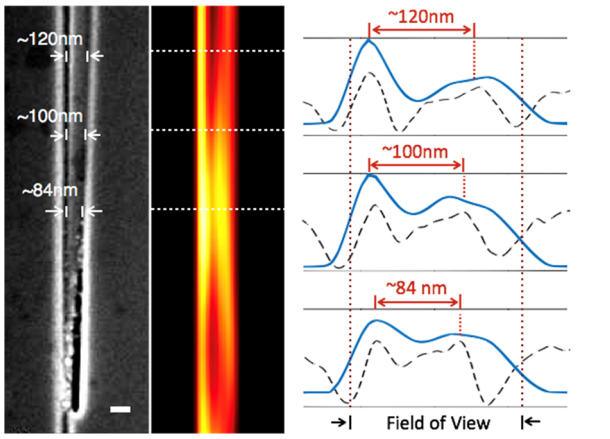

Figure 5. Super-resolution image demonstration. Left: SEM image of a tilted pair of slits milled into the Si_3N_4 layer. Slit width: ~35 nm. Middle: Super-resolution image. Right: Cross-section of the image at indicated locations. Blue solid line: Super-resolution image. Black dashed line: SEM image (inverted). Scale bar: 100 nm. The field of view is affected by the wavelength range of the hyperspectral image. Wavelength range: 460−700 nm.

image, the two slits gradually merge. A similar optical image is reconstructed. The intensity cross-section revealed that the hyperstructured illumination method can resolve down to ~84 nm, which is already close to the simulated FWHM of the tested multilayer system consisting of Ag−SiO_2 stacks (6 pairs; thickness of each layer, 14 nm). When the two slits are too close, it becomes a single deep slit milled into the HMM layer, which dramatically changes the dispersion relationship, causing a defect at the bottom part of the reconstructed optical image.

The imaging reconstruction forms a super-resolution image without knowing the exact shape of $E(x)$, which might be affected by HMM and the nanoslit quality and is hard to measure directly from the far field. Only the dispersion property of the HMM needs to be calibrated. It is worthy to note that wavelength dependence of the point spread function $\mathrm{PSF}(x, y)$ and pattern $E(x)$ is ignored in the above notations. In practice, the wavelength dependence will result in a spatially variant effective point spread function.

CONCLUSIONS

We studied a Ag/SiO_2 hyperbolic metamaterial to be used in a metamaterial-assisted illumination nanoscope (MAIN) with one-dimensional resolution improvement. By making artificial structures on both sides of the HMM, we characterize its material dispersion and show a 1D super-resolution image from a hyperspectral image acquired at the far field. This study shows that hyperstructured illumination is practically feasible, which provides an alternative method for nonfluorescent super-resolution surface imaging.

The resolution is mainly determined by the highest spatial-frequency wave the HMM can carry, and it is proportional to the unit pair size of the HMM multilayer.[17,24] For the Ag/SiO_2 system, a unit pair size of 20 nm is practically achievable by the sputtering method, which can bring the resolution down to ~50 nm. Other epitaxial growth metamaterial systems (*e.g.*, TiN/dielectric,[32] Ag/MgO[33]) that have a unit pair size down to a few nanometers can dramatically improve the resolution.

Another practical concern of imaging is the accuracies to estimate near-field illumination patterns. Distortion of near-field patterns happens when there is imperfections in the

DOI: 10.1021/acsnano.8b06026
ACS Nano XXXX, XXX, XXX−XXX

multilayer and nanofabrication. Fortunately, sophisticated reconstruction algorithms in structured illumination can reconstruct a super-resolution image without fully known illumination patterns, known as blind-SIM.[34] Research along this direction greatly reduces the strict requirement of knowing the exact near-field patterns and makes use of near-field patterns for structured illumination practically feasible.[22,23]

METHODS/EXPERIMENTAL

Software. We use COMOSL 4.1a to perform full wave simulation of a hyperbolic metamaterial and MATLAB 2017a to perform imaging reconstruction.

Experimental Setup. The sample is placed under a Zeiss inverted microscope. A supercontinuum laser (NKT Photonics, SuperK Extreme EXB-6), equipped with a tunable bandpass filter (NKT Photonics, SuperK VARIA tunable single line filter), is coupled to a microscope through a liquid light guide. A condenser (NA0.8) and a dark-field ring are used for dark-field illumination. The sample is imaged by a Zeiss 50×/0.5 objective lens. Hyperspectral images are acquired by an EMCCD (Andor iXon 897) by stepping the tunable bandpass filters.

HMM Preparation. The Si_3N_4 membrane window was purchased from SPI Supply Inc. (4104SN-BA). The Ag−SiO_2 multilayer and the top Cr layer are deposited by magnetron sputtering at room temperature (AJA International Inc.). All the nanoslits, including the single nanoslit on the Cr layer, the tilted single nanoslit on the Si_3N_4 layer, and the double slit on the Si_3N_4 layer, were fabricated by FEI Scios DualBeam at Nano3 facility at Calit2, UCSD.

ASSOCIATED CONTENT

Supporting Information

The Supporting Information is available free of charge on the ACS Publications website at DOI: 10.1021/acsnano.8b06026.

Figures of full wave simulation of normalized electrical field distribution for the Ag and SiO_2 multilayer; beam propagating angle *versus* wavelength for HMM made by the Ag/SiO_2 multilayer; raw camera frames of Figure 5 (PDF)

AUTHOR INFORMATION

Corresponding Author

*E-mail: zhaowei@ucsd.edu.

ORCID

Qian Ma: 0000-0002-7667-332X

Lorenzo Ferrari: 0000-0001-5313-8298

Xiang Zhang: 0000-0002-3272-894X

Notes

The authors declare no competing financial interest.

ACKNOWLEDGMENTS

This work was supported by the Gordon and Betty Moore Foundation and the National Science Foundation (CBET-1604216).

REFERENCES

(1) Betzig, E.; Patterson, G. H.; Sougrat, R.; Lindwasser, O. W.; Olenych, S.; Bonifacino, J. S.; Davidson, M. W.; Lippincott-Schwartz, J.; Hess, H. F. Imaging Intracellular Fluorescent Proteins at Nanometer Resolution. *Science* **2006**, *313*, 1642−1645.

(2) Rust, M. J.; Bates, M.; Zhuang, X. Sub-Diffraction-Limit Imaging by Stochastic Optical Reconstruction Microscopy (STORM). *Nat. Methods* **2006**, *3*, 793−795.

(3) Hess, S. T.; Girirajan, T. P. K.; Mason, M. D. Ultra-High Resolution Imaging by Fluorescence Photoactivation Localization Microscopy. *Biophys. J.* **2006**, *91*, 4258−4272.

(4) Hell, S. W.; Wichmann, J. Breaking the Diffraction Resolution Limit By Stimulated-Emission - Stimulated-Emission-Depletion Fluorescence Microscopy. *Opt. Lett.* **1994**, *19*, 780−782.

(5) Balzarotti, F.; Eilers, Y.; Gwosch, K. C.; Gynnå, A. H.; Westphal, V.; Stefani, F. D.; Elf, J.; Hell, S. W. Nanometer Resolution Imaging and Tracking of Fluorescent Molecules with Minimal Photon Fluxes. *Science* **2017**, *355*, 606−612.

(6) Gustafsson, M. G. L. Surpassing the Lateral Resolution Limit by a Factor of Two Using Structured Illumination Microscopy. *J. Microsc.* **2000**, *198*, 82−87.

(7) Li, D.; Shao, L.; Chen, B.-C.; Zhang, X.; Zhang, M.; Moses, B.; Milkie, D. E.; Beach, J. R.; Hammer, J. A.; Pasham, M.; Kirchhausen, T.; Baird, M. A.; Davidson, M. W.; Xu, P.; Betzig, E. Extended-Resolution Structured Illumination Imaging of Endocytic and Cytoskeletal Dynamics. *Science* **2015**, *349*, aab3500.

(8) Pendry, J. B. Negative Refraction Makes a Perfect Lens. *Phys. Rev. Lett.* **2000**, *85*, 3966−3969.

(9) Fang, N.; Lee, H.; Sun, C.; Zhang, X. Sub-Diffraction Limited Optical Imaging with a Silver Superlens. *Science* **2005**, *308* (5721), 534−537.

(10) Taubner, T.; Korobkin, D.; Urzhumov, Y.; Shvets, G.; Hillenbrand, R. Near-Field Microscopy through a SiC Superlens. *Science* **2006**, *313*, 1595.

(11) Liu, Z.; Lee, H.; Xiong, Y.; Sun, C.; Zhang, X. Far-Field Optical Hyperlens Magnifying Sub-Diffraction-Limited Objects. *Science* **2007**, *315*, 1686.

(12) Smolyaninov, I. I.; Hung, Y. J.; Davis, C. C. Magnifying Superlens in the Visible Frequency Range. *Science* **2007**, *315*, 1699−1701.

(13) Jacob, Z.; Alekseyev, L. V.; Narimanov, E. Optical Hyperlens: Far-Field Imaging Beyond the Diffraction Limit. *Opt. Express* **2006**, *14*, 8247−8256.

(14) Liu, Z.; Durant, S.; Lee, H.; Pikus, Y.; Fang, N.; Xiong, Y.; Sun, C.; Zhang, X. Far-Field Optical Superlens. *Nano Lett.* **2007**, *7*, 403−408.

(15) Rho, J.; Ye, Z.; Xiong, Y.; Yin, X.; Liu, Z.; Choi, H.; Bartal, G.; Zhang, X. Spherical Hyperlens for Two-Dimensional Sub-Diffractional Imaging at Visible Frequencies. *Nat. Commun.* **2010**, *1*, 143.

(16) Sun, J.; Shalaev, M. I.; Litchinitser, N. M. Experimental Demonstration of a Non-Resonant Hyperlens in the Visible Spectral Range. *Nat. Commun.* **2015**, *6*, 7201.

(17) Wood, B.; Pendry, J. B.; Tsai, D. P. Directed Subwavelength Imaging Using a Layered Metal-Dielectric System. *Phys. Rev. B: Condens. Matter Mater. Phys.* **2006**, *74*, 115116.

(18) Ferrari, L.; Wu, C.; Lepage, D.; Zhang, X.; Liu, Z. Hyperbolic Metamaterials and Their Applications. *Prog. Quantum Electron.* **2015**, *40*, 1−40.

(19) Kildishev, A. V.; Shalaev, V. M. Engineering Space for Light *via* Transformation Optics. *Opt. Lett.* **2008**, *33*, 43−45.

(20) Han, S.; Xiong, Y.; Genov, D.; Liu, Z.; Bartal, G.; Zhang, X. Ray Optics at a Deep-Subwavelength Scale: A Transformation Optics Approach. *Nano Lett.* **2008**, *8*, 4243−4247.

(21) Ma, Q.; Liu, Z. Metamaterial-Assisted Illumination Nanoscopy. *Natl. Sci. Rev.* **2018**, *5*, 141−143.

(22) Wei, F.; Lu, D.; Shen, H.; Wan, W.; Ponsetto, J. L.; Huang, E.; Liu, Z. Wide Field Super-Resolution Surface Imaging through Plasmonic Structured Illumination Microscopy. *Nano Lett.* **2014**, *14*, 4634−4639.

(23) Ponsetto, J. L.; Bezryadina, A.; Wei, F.; Onishi, K.; Shen, H.; Huang, E.; Ferrari, L.; Ma, Q.; Zou, Y.; Liu, Z. Experimental Demonstration of Localized Plasmonic Structured Illumination Microscopy. *ACS Nano* **2017**, *11*, 5344−5350.

(24) Narimanov, E. Hyperstructured Illumination. *ACS Photonics* **2016**, *3*, 1090−1094.

DOI: 10.1021/acsnano.8b06026
ACS Nano XXXX, XXX, XXX−XXX

(25) Ma, Q.; Hu, H.; Huang, E.; Liu, Z. Super-Resolution Imaging by Metamaterial-Based Compressive Spatial-to-Spectral Transformation. *Nanoscale* **2017**, *9*, 18268−18274.
(26) Zeng, X.; Al-Amri, M.; Zubairy, M. S. Nanometer-Scale Microscopy *via* Graphene Plasmons. *Phys. Rev. B: Condens. Matter Mater. Phys.* **2014**, *90*, 235418.
(27) Ertsgaard, C. T.; McKoskey, R. M.; Rich, I. S.; Lindquist, N. C. Dynamic Placement of Plasmonic Hotspots for Super-Resolution Surface-Enhanced Raman Scattering. *ACS Nano* **2014**, *8*, 10941−10946.
(28) Cang, H.; Liu, Y.; Wang, Y.; Yin, X.; Zhang, X. Giant Suppression of Photobleaching for Single Molecule Detection *via* the Purcell Effect. *Nano Lett.* **2013**, *13*, 5949−5953.
(29) Segovia, P.; Marino, G.; Krasavin, A. V.; Olivier, N.; Wurtz, G. A.; Belov, P. A.; Ginzburg, P.; Zayats, A. V. Hyperbolic Metamaterial Antenna for Second-Harmonic Generation Tomography. *Opt. Express* **2015**, *23*, 30730.
(30) Ishii, S.; Kildishev, A. V.; Narimanov, E.; Shalaev, V. M.; Drachev, V. P. Sub-Wavelength Interference Pattern from Volume Plasmon Polaritons in a Hyperbolic Medium. *Laser Photonics Rev.* **2013**, *7*, 265−271.
(31) York, A. G.; Parekh, S. H.; Nogare, D. D.; Fischer, R. S.; Temprine, K.; Mione, M.; Chitnis, A. B.; Combs, C. A.; Shroff, H. Resolution Doubling in Live, Multicellular Organisms *via* Multifocal Structured Illumination Microscopy. *Nat. Methods* **2012**, *9*, 749−754.
(32) Hoffman, A. J.; Alekseyev, L.; Howard, S. S.; Franz, K. J.; Wasserman, D.; Podolskiy, V. A.; Narimanov, E. E.; Sivco, D. L.; Gmachl, C. Negative Refraction in Semiconductor Metamaterials. *Nat. Mater.* **2007**, *6*, 946−950.
(33) Velázquez, D.; Seibert, R.; Yusof, Z.; Terry, J.; Spentzouris, L. Synthesis of Ultra-Thin Single Crystal MgO/Ag/MgO Multilayer for Controlled Photocathode Emissive Properties. *International Particle Accelerator Conference* **2015**, 1846−1849.
(34) Mudry, E.; Belkebir, K.; Girard, J.; Savatier, J.; Le Moal, E.; Nicoletti, C.; Allain, M.; Sentenac, A. Structured Illumination Microscopy Using Unknown Speckle Patterns. *Nat. Photonics* **2012**, *6*, 312−315.

DOI: 10.1021/acsnano.8b06026
ACS Nano XXXX, XXX, XXX−XXX